Efficiently electrochemical removal of nitrite contamination with stable RuO_2-TiO_2/Ti electrodes

Huan Yue, Lingzhi Xue, Feng Chen[*]

Key Laboratory for Advanced Materials and Institute of Fine Chemicals, East China University of Science and Technology, 130 Meilong Road, Shanghai, 200237, China

ABSTRACT

RuO_2-TiO_2/Ti electrode was prepared for the electrocatalytic removal of nitrite in this work. The influences of calcination temperatures on crystal phase and morphology of RuO_2-TiO_2 composite were explored by XRD and TEM. The formation of RuO_2 epitaxial layers on the surface of TiO_2 by calcination at 400 °C reduces the impedance (EIS test) and improves the electrocatalytic activity for RuO_2-TiO_2. The CV test shows that the electrochemically surface active sites increase along with the increase of RuO_2 content from 0 to 2.0 wt%. The nitrite removal rate of 2.0 wt% RuO_2-TiO_2/Ti electrode is found ca. 6.7 and 2.5 times faster than those of 0.02 wt% and 0.1 wt% RuO_2-TiO_2/Ti electrodes, respectively. Oxidation of the active sites on the RuO_2 results in an obvious activity decrease for RuO_2/Ti and RuO_2-TiO_2/Ti electrodes in just 3 reaction cycles (30 min/cycle). By exchanging the anode and cathode after every cycle, the catalytic activity of corresponding 2.0 wt% RuO_2-TiO_2/Ti electrode remains almost unchanged after 50 cycles. Although the electrocatalytic service life of RuO_2/Ti electrode is also greatly improved, its electrocatalytic activity decreases much after 50 cycles. The relatively longer service life of 2.0 wt% RuO_2-TiO_2/Ti electrode should own to the intensified interaction between the epitaxially spread RuO_2 and TiO_2, which stabilizes the chemical states of RuO_2. The main product for the electrocatalytic removal of nitrite is nitrate by indirect oxidation, while a small amount of ammonium is also produced at the cathode. The as-produced ammonium will be oxidized into nitrogen molecule, which is released from the aqueous solution afterwards and contributes the decrease of the total content of N in the solution.

© 2017 Elsevier B.V. All rights reserved.

1. Introduction

Nitrite (NO_2^-) contamination in water resources has received particularly environmental concerns, as it causes serious human health problems like liver damage, blue baby syndrome and cancers [1,2]. To safeguard people's health, the concentration of NO_2^- over 0.5 mg L^{-1} in drinking water is not allowed [3]. Many conventional treatments, such as physical-chemical adsorption with activated carbon [4], biological processes [5], and chemical oxidation with oxidants [6] are adopted to remove nitrite from the water. However, high costs, secondary pollution, low running efficiency, and other disadvantages prevent them from applying effectively in many cases [4–7]. To avoid these shortages, electrochemical catalysis is recommended as an environmental-friendly progress. Generally, it can be easily operated, feasible to be auto-

mated process, and low cost. Nowadays, electrochemistry method is increasingly applied in the wastewater treatment. Electrochemical oxidation can effectively oxidize nitrite ion [8] and organic pollutants in aqueous solution by direct or indirect oxidation [9]. Several electrode materials, such as SnO_2/Ti [10], RuO_2/Ti [11], IrO_2/Ti [12] and boron-doped diamond [13], have been used for the electrolytic treatment processes, of which the electrodes are composed of transition metal oxides. The M_1O_x-M_2O_x/Ti electrodes used in these cases are called dimensionally stable anodes (DSA), which gives more advanced performances (catalytic activity, stability and low cost) than those of conventional anodes (metal, carbon, etc) [14–17]. Generally, indirectly electrochemical oxidation [18] is suggested as the main process that occurs in the electrolytic wastewater treatment, in which an anodic electrocatalysis leads to the generation of hydroxyl radicals (OH•) or active chlorine species (ClO$^-$) in the presence of chloride ion [19]. Specifically, most of DSA electrodes (SnO_2-Sb/Ti [20], PbO_2/Ti [21]) tend to produce OH• to oxidized pollutants, while RuO_2-TiO_2/Ti electrode and IrO_2-TiO_2/Ti [22] are prone to produce ClO$^-$.

* Corresponding author.
E-mail addresses: helenyue668@163.com (H. Yue), zhilingxue@163.com (L. Xue), fengchen@ecust.edu.cn (F. Chen).

Based on the isomorphism rule, ions of the same type with similar ionic radius can co-exist in the same lattice. Accordingly, the ionic radius of Ru^{4+} and Ti^{4+} are 0.065 nm and 0.064 nm, respectively; therefore, RuO_2 and TiO_2 could form a solid solution and give strong junction at their interface [23], which brings the RuO_2-TiO_2/Ti electrode excellent electric conductivity. Consequently, RuO_2-TiO_2/Ti electrode is effectively applied in the chlor-alkali processes for its low chlorine evolution potential, relatively high oxygen evolution potential and excellent electric conductivity [24,25]. However, the further applications of the RuO_2-TiO_2/Ti electrode are limited by the short service life in anodic polarization conditions and the occurrence of the coating shedding [23,24,26]. Our work aims to evaluate the electrocatalytic performance and the electrochemical stability of RuO_2-TiO_2/Ti electrode during the nitrite removal process, as well as the relationship between chemical state and electrochemical activities of RuO_2-TiO_2 composite. In addition, the electrochemical nitrite-N removal mechanism is suggested according to the experimental observations.

2. Experimental section

2.1. Reagents and materials

TiO_2 (P25, Evonik Degussa), $RuCl_3$ (AR) were obtained from commercial sources. NaCl, $NaNO_2$, KNO_3, Na_2SO_4 and NH_4Cl were obtained from Sinopharm Chemical Reagent. All the reagents were AR and used as received. Ultrapure water (18.2 MΩ) was used throughout the work.

2.2. Preparation of RuO_2-TiO_2/Ti electrode

2.2.1. Synthesis of RuO_2-TiO_2 composite

A hydrothermal method was used to prepare RuO_2-TiO_2 composite just as our previous report [27]. A desired amount of $RuCl_3$ was mixed with the specified amount of TiO_2 in different ratios (0 wt%, 0.02 wt%, 0.1 wt%, 2.0 wt%, 100 wt%) using water as the solvent to ensure a total volume of 75 mL. Then the mixture was transferred into a 100 mL autoclave and heated at 180 °C for 10 h. After cooling down, the product was separated by centrifuging, washed with water for three times, and dried at 60 °C under vacuum overnight to get the RuO_2-TiO_2 catalysts.

2.2.2. Electrode preparation

The electrode was prepared from titanium plate with 0.50 mm thickness. The titanium plate (4.0 cm × 7.5 cm) was first degreased in 0.50 M NaOH aqueous solution at 60 °C for 30 min, then washed with water and sonicated in ethanol for 30 min. Next, it was polished with 1000-mesh emery paper and etched in 10 wt% boiling oxalic acid solution for 2.5 h [23]. Then, the titanium plate was washed with water, sonicated for 15 min, and dried for use.

The painting suspension was prepared by dispersing the above-prepared RuO_2-TiO_2 composite in ethanol under ultrasonic condition. Then the prepared painting suspension was pasted to the pretreated titanium plates (4.0 cm × 7.5 cm) with a brush. The painted Ti plate was then dried at 100 °C for 10 min. In the same way, the other side of the titanium plate was also coated. The coating process was repeated for several times to load a desired amount of catalysts. The total mass of the deposited composite was fixed to 0.04 g for each side. Finally, the plate was calcined under the desired temperature (200 °C, 300 °C, 400 °C, 500 °C, and 600 °C) for 10 h to obtain a RuO_2-TiO_2/Ti active electrode.

2.3. Catalyst characterization

The crystalline structure of RuO_2-TiO_2 catalysts was measured by X-ray diffraction (XRD). Diffraction patterns of the samples were performed using an X-Ray diffractometer (Rigaku Ultima IV) operating in the reflection mode with Cu Kα radiation. A continuous scan mode was employed to collect 2θ data from 10° to 80° with a scan step of 0.02°. Transmission electron microscopy (TEM) was investigated using a JEOL JEM 2100F instrument operated at 200 kV. The morphologies of the samples were pictured with SEM (Tescan VEGA 3 SBU) observation. The chemical compositions of samples were analyzed by X-ray photoelectron spectroscopy (XPS, Thermo Fisher ESCALAB 250Xi system with Al Kα radiation), and calibrated internally by carbon deposit C1s binding energy (BE) at 284.6 eV.

2.4. Electrochemical measurements

The electrochemical properties of RuO_2-TiO_2 electrodes were analyzed through cyclic voltammetry (CV), polarization tests and electrochemical impedance spectroscopy (EIS). The electrochemical measurements were carried out in a three-electrode system (electrochemical workstation, Zahner Co., Germany) with a Pt electrode as the counter electrode, a Saturated Calomel Electrode (SCE) as the reference electrode, and RuO_2-TiO_2/Ti electrode as the working electrode. The effective working area of the electrode was 4.0 cm × 5.5 cm. The electrolytes for polarization tests were 0.05 M NaCl (for chlorine evolution potential test) and 0.0167 M Na_2SO_4 aqueous solution (for oxygen evolution potential test). The CV tests were carried out in 0.05 M NaCl and 10 ppm $NaNO_2$ aqueous solution. Cyclic voltammograms were recorded between −3.0 and $3.0 V_{SCE}$ at a scan rate of 100 mV s^{-1}. The EIS spectra of electrode materials were analyzed by using 2.5 mM $K_3Fe(CN)_6$/$K_4Fe(CN)_6$ (1:1) and 1.0 M KCl aqueous solution as the electrolyte. The frequency ranged from 0.01 Hz to 10 MHz and the amplitude of the potential was 3.0 V. The measured EIS data were analyzed and fitted to the equivalent electrical circuits by ZSimpWin software.

2.5. Electrocatalytic removal of nitrite

A DC potentiostat (APS3005DM, ATTEN instrument, China) was employed as the power supply for electrochemical reactions. Synthetic nitrite solution at a concentration of 10 mg L^{-1} $NaNO_2$ was used. The volume of each solution with 0.05 M NaCl for electrochemical test was 250 mL. The RuO_2-TiO_2/Ti electrodes were used as both the anode and cathode, which were placed vertically in parallel in the reactor with a gap of 1.0 cm. The immersed areas of the anodes and cathodes in the treated solution were both 4.0 cm × 5.5 cm. The applied voltage was fixed at 5.0 V. Unless specially stated, all the tests were carried out at room temperature (25 °C).

2.6. Analysis of aqueous N-species

Generally, the main aqueous soluble N-products in this work are nitrate, nitrite and ammonia. Nitrate-N and ammonia-N were measured by an ionometer (PXS-270, Shanghai INESA Scientific Instrument) with ion selectivity electrodes (PNO3-1-01, PNH3-1-01, Shanghai INESA Scientific Instrument), whereas nitrite-N was analyzed with a colorimetric method on an ultraviolet-visible spectrophotometer (UV-2600, Shimadzu). According to the fact that the NO_2^- forms red dye when coupling with sulfanilamide, the NO_2^- concentration can be analyzed by measuring the absorbance of red dye at the wavelength of 540 nm [28]. Briefly, 2.5 mL sample solution and 1 mL sulfanilamide were added into a 50 mL volumetric flask. Then the solution was adjusted to pH 1.8 by phosphoric acid, and diluted with water to a volume of 50 mL. After 30 min, the as-prepared red solution was analyzed by recording variations of the absorbance at 540 nm with a UV-2600.
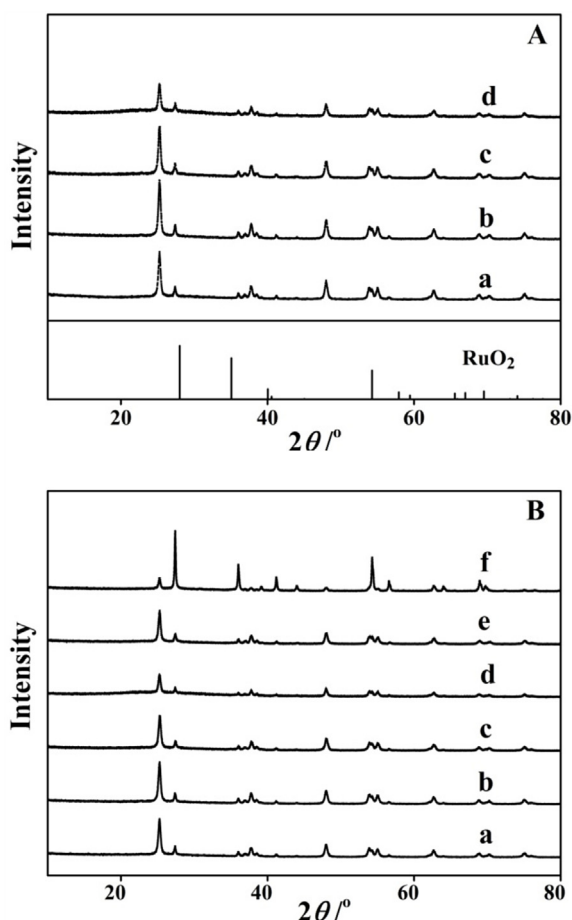
Fig. 1. (A) XRD patterns of (a) P25, (b) 0.02 wt% RuO_2-TiO_2, (c) 0.1 wt% RuO_2-TiO_2, and (d) 2.0 wt% RuO_2-TiO_2 calcined at 400 °C; (B) XRD patterns of (a) raw 2.0 wt% RuO_2-TiO_2 and 2.0 wt% RuO_2-TiO_2 calcined at (b) 200 °C, (c) 300 °C, (d) 400 °C, (e) 500 °C, and (f) 600 °C.

Fig. 2. (A) Ru 3d and (B) Ti 2p XPS fine spectra of (a) 2.0 wt% RuO_2-TiO_2 composite calcined at 400 °C, and (b) pristine RuO_2. *The XPS intensity for pristine RuO_2 was reduced 5 times.

3. Results and discussion

3.1. Crystal phase and morphology of catalysts

Fig. 1A displays the XRD signals of RuO_2-TiO_2 composite with different mass ratios of RuO_2. The relative contents of anatase and rutile for P25 TiO_2 can be estimated with the integral area ratios of their signals at 25.2° and 27.3°, respectively. P25 TiO_2 is composed of anatase (80%) and rutile (20%), which is consistent with the literature reports [27]. No XRD signal for RuO_2 is observed even at the highest RuO_2 content of 2.0 wt%. The as-prepared RuO_2-TiO_2 composite gives typical XRD signals as those of P25 TiO_2. The absence of the characteristic peak for RuO_2 should be due to the low content of RuO_2 in the composite. As thermal treatment possibly changes the crystal phase of the metal oxides, the crystal structures of RuO_2-TiO_2 composites calcined under various temperatures were also investigated with XRD measurements (Fig. 1B). It shows that calcination at temperatures below 400 °C have no obvious effect on the crystalline phase of TiO_2. However, the phase transition from anatase into rutile begins to occur when the composite was calcined at temperature above 500 °C. As is shown in Fig. 1B, the relative content of rutile increases a little after calcined at 500 °C, while the rutile phase becomes the dominant phase of the composite after calcined at 600 °C. Since the occurrence of RuO_2 in the composite cannot be verified with the XRD observation, the presence of ruthenium species was identified with XPS spectroscopy. Fig. 2 shows XPS fine spectra of Ru 3d (C 1s) and Ti 2p orbits of 2.0 wt% RuO_2-
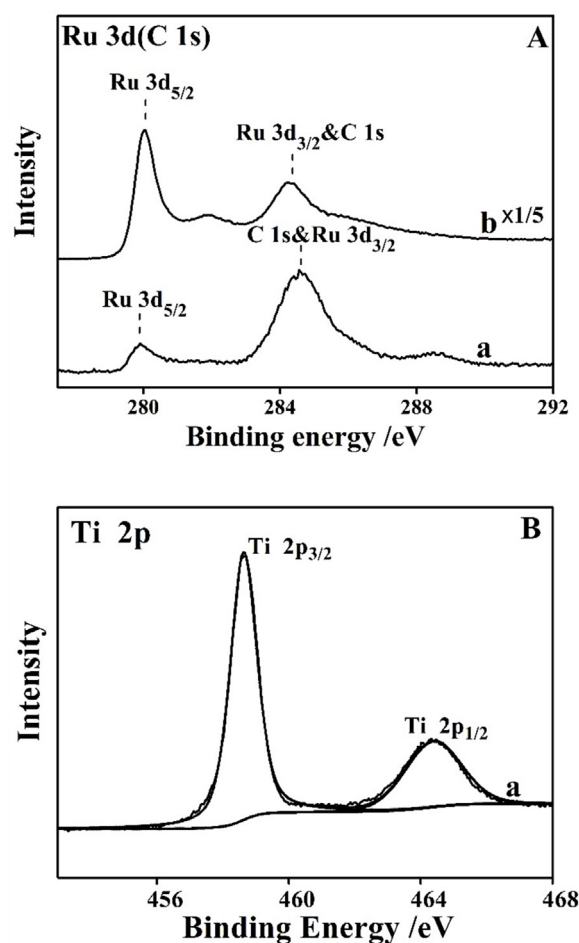
TiO_2 composite calcined at 400 °C. For reference, Ru 3d (C 1s) XPS fine spectrum of a pristine RuO_2 (Fig. S1 for XRD data) prepared with a thermal decomposition method [29] was also presented. The signals with binding energy over 283.0 eV for RuO_2-TiO_2 composite in Fig. 2A mainly belong to the C 1s signals. The emergence of the element C here should be due to the extrinsic contaminants from the C-adhesives during the sample fabrication process. Generally, the signal for the Ru $3d_{3/2}$ photoelectrons [30,31] is estimated to be located at ~284.4 eV as shown in that for pristine RuO_2, which is however overlapped with the strong C1 s peak at 284.6 eV and cannot be well identified for RuO_2-TiO_2 composite in Fig. 2A; hence, the presence and the chemical state of Ru for the composite is mainly identified from the signals of Ru $3d_{5/2}$ signals. As is shown in Fig. 2A, the signals around the binding energy of ~280.0 eV is ascribed to the Ru $3d_{5/2}$ signals of Ru(IV) [31–34] and can be used to verify the presence of RuO_2. The XPS signals of Ti (Fig. 2B) give two peaks in the Ti 2p region: one centered at 458.5 eV belongs to Ti $2p_{3/2}$, while another one is the signal of Ti $2p_{1/2}$ at 464.2 eV. It suggests the presence of Ti(IV) in the RuO_2-TiO_2 composite [31,35]. Briefly, the composite is composed of RuO_2 and TiO_2 according to the XPS observation.

The presence and the changes of RuO_2 on the surface of TiO_2 can be further verified with TEM observation (Fig. 3). Before the calcination, a great amount of RuO_2 nanoclusters can be observed as dark dots on the surface of TiO_2 for raw RuO_2-TiO_2 composite (Fig. 3A). After being calcined at 400 °C in air, RuO_2 nanoclusters disappear for the calcined RuO_2-TiO_2 composite (Fig. 3B). It should be due to
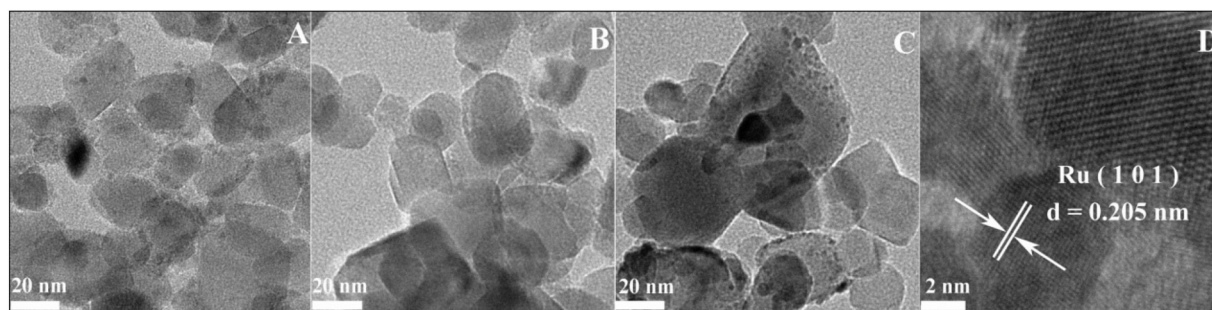
Fig. 3. The TEM images of RuO_2-TiO_2 composite (A) raw, (B) calcined at 400 °C in air, and (C&D) Ru^0-TiO_2 composite. *Ru^0-TiO_2 composite was obtained by calcining raw RuO_2-TiO_2 composite at 400 °C in air for 10 h, and then 400 °C in H_2 for 3 h.

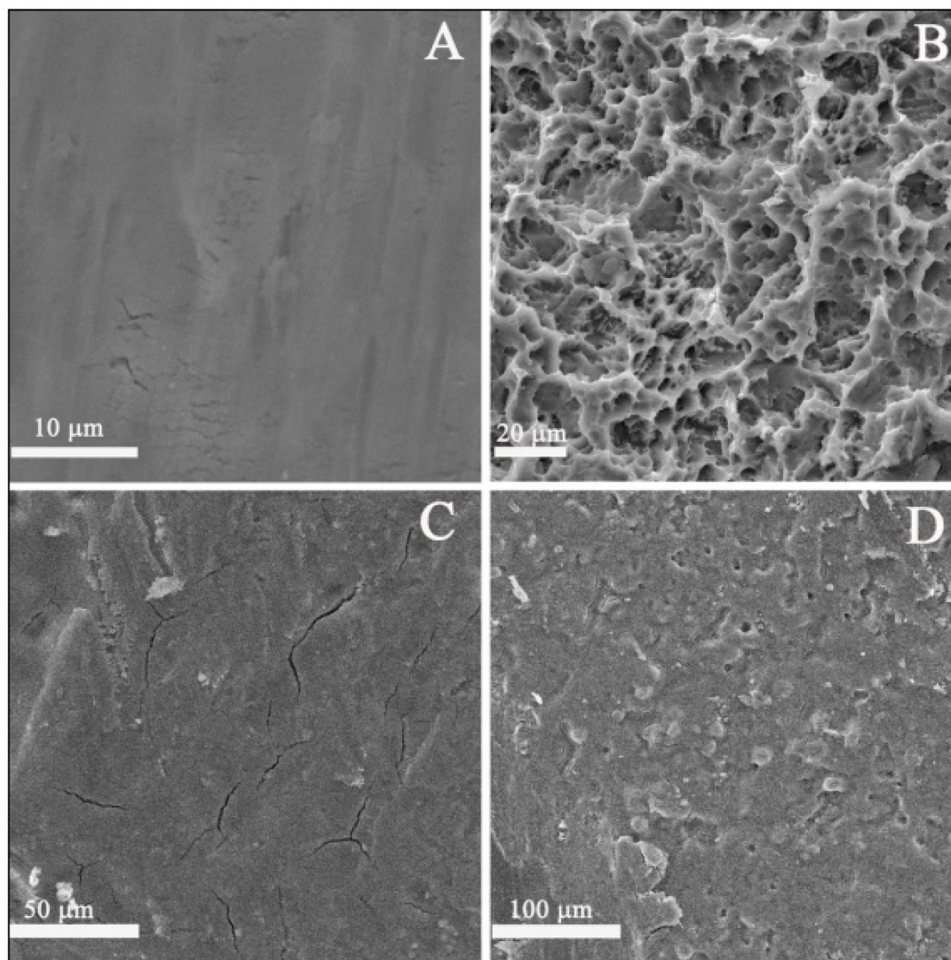**Fig. 4.** SEM images of (A) raw Ti plate, (B) Ti plate after acid etched (10% oxalic acid, 85 °C, 2.5 h), and (C, D) RuO_2-TiO_2 coated Ti plate.

the epitaxial growth of RuO_2, which makes RuO_2 nanoclusters into very thin membrane and invisible with TEM observation. Literature works reported [27,36] that the small RuO_2 nanoparticles can epitaxially grow along with the surface of TiO_2 after calcinations at 400 °C in air. When the composite is further calcined in H_2 at 400 °C, the small dark dots appear again in the TEM (Fig. 3C). The re-emerged dots are assigned as the metallic Ru^0 clusters, according to its characteristics lattice fringe of 0.205 nm (Fig. 3D). The metallic Ru^0 has less interaction with the TiO_2 lattice and thus cannot maintain an epitaxial morphology as that of RuO_2. In addition, the epitaxial growth of RuO_2 on the surface of TiO_2 can also be partially verified from the XPS observation of RuO_2-TiO_2 composites after calcination under various temperatures (Fig. S2).

3.2. Morphology of the RuO_2-TiO_2/Ti electrode

The factors that affect the electrochemical performance and structural stability of the RuO_2-TiO_2/Ti electrode have arisen widespread concern for a long time [23,24,26,37,38], but the stability problems still exist for practical application. It is generally believed that the main causes of DSA electrode deactivation are [26,37,39–42]: (1) the active oxides falling off from the Ti substrate, on account of the weak attachment between the Ti substrate and active oxides; (2) the newly produced oxygen permeating into the Ti substrate through cracks on the surface of electrodes during the electrochemical process, which leads to the passivation of Ti substrate; (3) the decrease of active sites (oxygen vacancies), as the
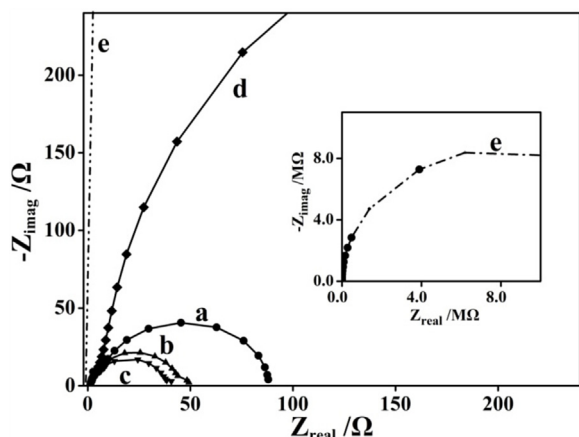
Fig. 5. A Nyquist plot of RuO_2-TiO_2/Ti electrodes calcined at temperatures of (a) 200 °C, (b) 300 °C, (c) 400 °C, (d) 500 °C, and (e) 600 °C in 2.5 mM $K_3Fe(CN)_6$/$K_4Fe(CN)_6$(1:1) and 1 M KCl at a potential of $3.0 V_{SCE}$. Inset shows the Nyquist plot of electrode calcined at 600 °C.
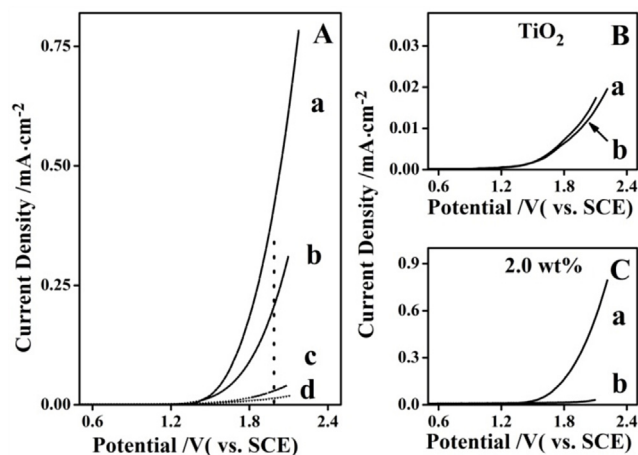

Fig. 6. (A) The polarization curves of (a) 2.0 wt% RuO_2-TiO_2/Ti, (b) 0.1 wt% RuO_2-TiO_2/Ti, (c) 0.02 wt% RuO_2-TiO_2/Ti, and (d) TiO_2/Ti electrodes in 0.05 M NaCl solution. And the polarization curves of (B) TiO_2/Ti electrodes and (C) 2.0 wt% RuO_2-TiO_2/Ti electrodes in (a) 0.05 M NaCl solution and (b) 0.0167 M Na_2SO_4 solution.

Ru(IV) from the dioxide easily form unstable tetraoxide at high electrical potential.

For the first issue, the pre-treatment of Ti substrate with oxalic acid etching was carried out to strengthen the adhesion of RuO_2-TiO_2 to the Ti substrate. Fig. 4 presents the SEM images of the raw Ti plate, oxalic acid etched Ti plate and RuO_2-TiO_2 coated Ti plate. After the treatment of oxalic acid, the surface profile of Ti plate changes obviously from a relatively smooth to a highly porous manner. Supposedly, porous TiH_x component is formed at the surface of Ti substrate during the oxalic acid treatment (Fig. S3) [23,43]. Then TiH_x is oxidized into Ti and TiO_2 to fabricate a porous TiO_2 skin at the surface of Ti plate. The highly porous surface structure with a TiO_2 skin is beneficial to increase the interaction between the coating layer and the Ti substrate, as well as magnifies the actual surface of Ti substrate. With the assistance of the TiO_2 skin, the coated RuO_2-TiO_2 layers can penetrate well into the porous structure and bind tightly to the Ti substrate.

3.3. The electrochemical properties of electrodes

Nevertheless, the challenges from the active oxygen still exist. For instance, the active oxygen in-situ produced during the electrochemical reaction possibly induces the oxidation of Ti substrate and
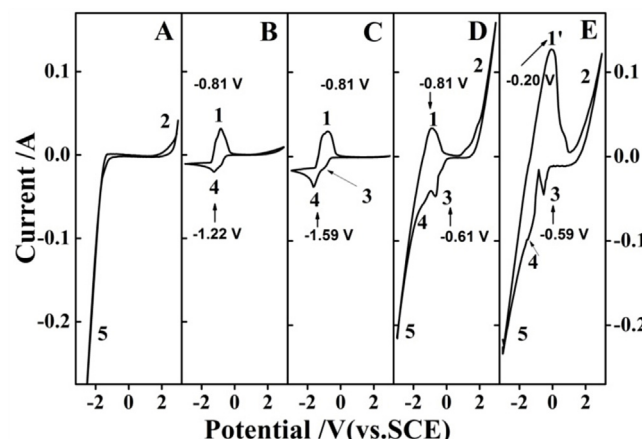
thus passivates the electrode [23]. Accordingly, increasing the oxygen evolution potential would be an effective way to improve the stability of the electrode. Therefore, the electrochemical properties of the RuO_2-TiO_2/Ti electrode were observed in detail.

3.3.1. EIS spectroscopy

Fig. 5 shows the EIS results of RuO_2-TiO_2/Ti electrodes calcined at various temperatures for 10 h. Calcination treatment has an obvious impact on the electrochemical properties of electrodes. Initially, the electrical resistance of RuO_2-TiO_2/Ti electrodes decreases gradually with the increase of calcination temperature and reaches its minimum at 400 °C. However, further increasing calcination temperature causes a significant increase of impedance. Corresponding to the changes from XRD and TEM results, the RuO_2 grains here should epitaxially grow along with the surface of anatase when calcined at temperatures above 400 °C. However, a phase transition of TiO_2 begins to occur at calcination temperatures above 500 °C and the rutile phase even becomes the dominant phase of the composite after calcination at 600 °C. Since rutile has higher electric resistance than that of anatase, such a phase transition is seriously adverse for decreasing the electrical resistance of the composite.

3.3.2. Polarization curve

As is shown in Fig. 6A, the increasing amount of RuO_2 in RuO_2-TiO_2 composite gradually decreases the chlorine evolution potential; meanwhile, the anodic current becomes much higher with the higher RuO_2 content at the same applied voltage. It could be seen in Fig. 6B and C that the potential difference between chlorine and oxygen evolution potential is getting larger than that of the bare TiO_2 after the load of 2.0 wt% RuO_2. Loading a certain amount of RuO_2 can not only improve the electrical conductivity and catalytic efficiency, but also decrease the possibility of the electrode oxidation by active oxygen, thus enhancing the electrochemical stability of electrodes.

3.3.3. CV test

Fig. 7 shows the CV test obtained on the RuO_2-TiO_2/Ti electrodes in a 0.05 M NaCl aqueous solution. Peaks 4 and 1 are the red/ox signals of oxygen vacancies in TiO_2, while peaks 3 and 1′ are the red/ox signals of oxygen vacancies in RuO_2 in the reverse sweep from 3.0 V to −3.0 V and the forward sweep from −3.0 V to 3.0 V. The oxygen vacancies which are positive charge in TiO_2 would gain electrons when the applied voltage is below −1.22 V versus SCE (peak 4), that is, Ti^{3+} species get restored. Inversely, the reduced oxygen vacancies (Ti^{3+} species) lose electrons and be oxidized when the applied

Fig. 7. Cyclic voltammograms of (A) Ti, (B) TiO_2/Ti, (C) 0.02 wt% RuO_2-TiO_2/Ti, (D) 0.1 wt% RuO_2-TiO_2/Ti, and (E) 2.0 wt% RuO_2-TiO_2/Ti electrodes obtained in a 0.05 M NaCl at scan rate 100 mV s^{-1}.

voltage increases up to -0.81 V (peak 1, the anodic peak of oxygen vacancies in TiO_2). With the increase of the RuO_2 loading amount, the positions and shapes of peaks 1, 3 and 4 change a little. Particularly, when the loading amount is 2.0 wt%, a new and much stronger peak (peak 1′) appears at higher potential of -0.20 V (Fig. 7E), while the oxidation of reduced oxygen vacancies (Ru^{3+}) in RuO_2 gives an intensified cathodic signal (peak 3, -0.59 V). Due to the overlap of the peak 1′, the peak 1 cannot be clearly observed in Fig. 7E. Furthermore, the peak 2 stands for chlorine evolution peak and peak 5 is hydrogen evolution peak. An enhanced catalytic performance of RuO_2-TiO_2 can be concluded from the increased peak areas of its corresponding current for chlorine evolution (peak 2). Meanwhile, as for hydrogen evolution (peak 5), we can see that better conductivity results in a higher hydrogen evolution rate and potential. As is shown in Fig. 7A, Ti plate is the best for the hydrogen evolution while P25 covered Ti plate gives the lowest hydrogen evolution. Generally, integration of the I-E curve provides the voltammetric charge, which is suggested to proportional to the number of electrochemically surface active sites [44]. With the increase of the RuO_2 loading amount, the voltammetric charge on the RuO_2-TiO_2/Ti electrode gradually increase, which contributes to excellent electrical conductivity and diffusion barrier properties of RuO_2 [31], as well as the increase of whole surface active sites of the RuO_2-TiO_2/Ti electrode. That is to say, adding appropriate amount of RuO_2 would help to improve the conductivity and electrocatalytic efficiency of the RuO_2-TiO_2/Ti electrode.

3.4. Performance of RuO_2-TiO_2/Ti electrodes for the removal of nitrite

To investigate the electrocatalytic efficiency of the different RuO_2-TiO_2/Ti electrodes, the nitrite electrocatalytic removal was performed as a test reaction. Fig. 8A shows that RuO_2 is more effective in nitrite removal than TiO_2. The electrochemical activity of electrode improves obviously even with a low concentration RuO_2 of 0.02 wt%. For Ti electrode, TiO_2/Ti electrode, and 0.02 wt% RuO_2-TiO_2/Ti electrode, the removal rates for nitrite are 2.6% (curve a), 18.9% (curve b), 99.7% (curve c) in 1 h. The reactivity of electrode greatly increases with the increasing amount of loaded RuO_2. For the fact that the nitrite removal rate of RuO_2-TiO_2/Ti electrodes with RuO_2 loading amount above 0.1 wt% within 5 min comes to 100%. Specifically, the nitrite removal rate of 2.0 wt% RuO_2-TiO_2/Ti electrode is ca. 6.7 times and ca. 2.5 times faster than that of 0.02 wt% RuO_2-TiO_2/Ti and 0.1 wt% RuO_2-TiO_2/Ti electrodes, respectively. Meanwhile, pure RuO_2/Ti electrode (curve f) shows as high electrocatalytic activity as that of 2.0 wt% RuO_2-TiO_2/Ti for nitrite removal. In summary, adding appropriate amount of RuO_2 would greatly help to improve the electrochemical efficiency of the RuO_2-TiO_2/Ti electrode.

The results in Fig. 8B show that the electrocatalytic nitrite removal performances of the 2.0 wt% RuO_2-TiO_2/Ti electrode reach its optimum condition when the electrode was calcined at 400 °C. That for the RuO_2-TiO_2/Ti calcined at 300 °C is slightly worse. The nitrite removal rates with RuO_2-TiO_2/Ti calcined at 200 °C, 300 °C, 400 °C are 14.8%, 81.3%, 90.3% in 1 min, respectively. However, when the calcination temperature is above 400 °C, the performances of the electrode become to deteriorate. Specifically, the nitrite removal rates with RuO_2-TiO_2/Ti electrode calcined at 400 °C is ca. 15.0 times faster than that with RuO_2-TiO_2/Ti calcined at 500 °C. Only 57.4% and 1.7% of nitrite were removed in 20 min with the electrodes calcined at 500 °C and 600 °C, respectively. It gives a similar trend with the results of electrochemical impedance, of which the electrical resistance of RuO_2-TiO_2/Ti electrodes reaches its minimum at 400 °C (Fig. 5). Supposedly, the smaller the impedance, the better the electrocatalytic performance is. It is observed that calcination is the decisive step in the phase
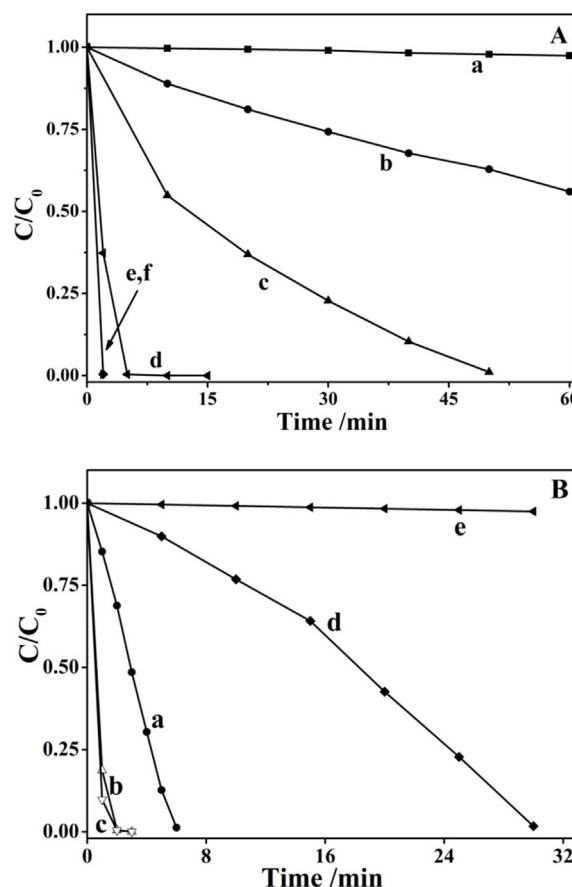

Fig. 8. (A) Electrocatalytic nitrite removal with (a) Ti, (b) TiO_2/Ti, (c) 0.02 wt% RuO_2-TiO_2/Ti, (d) 0.1 wt% RuO_2-TiO_2/Ti, (e) 2.0 wt% RuO_2-TiO_2/Ti and (f) RuO_2/Ti (overlaps with curve e) electrodes; (B) Electrocatalytic nitrite removal with 2.0 wt% RuO_2-TiO_2/Ti electrodes calcined at temperatures of (a) 200 °C, (b) 300 °C, (c) 400 °C, (d) 500 °C, and (e) 600 °C.

transition of TiO_2 (Fig. 1B) as well as epitaxial structure formation of the RuO_2-TiO_2 composites (Fig. 3), which influence the impedance of RuO_2-TiO_2/Ti electrode. The electrochemical impedance is one important parameter for valuing the performances of the electrode materials, while calcination temperature determines the impedance, so it is concluded that the electrochemical activity of electrode is closely related to the calcinations. The optimal calcinations temperature of RuO_2-TiO_2/Ti electrode is 400 °C as observed.

3.5. Long-term work of the electrode

In order to investigate the electrochemical stability of RuO_2-TiO_2/Ti electrode, the 30 min electrocatalytic treatment of nitrite (10 mg L^{-1} $NaNO_2$) was repeatedly operated. The reproducibility of the nitrite removing is pretty bad when RuO_2-TiO_2/Ti electrode and RuO_2/Ti were fixedly and merely used as the anodes (Fig. 9A, C and E). The performances of RuO_2-TiO_2/Ti (0.1 wt%, 2.0 wt%) and RuO_2/Ti decrease apparently after the continuous service of 90 min (3 cycles). As discussed previously, the active site of RuO_2-TiO_2 composites is easily oxidized in anodic polarization conditions [23,24,26]. The CV observation (Fig. 7) suggests that the active sites of RuO_2-TiO_2 composites would experience a redox cycle in one CV scan cycle. Therefore, an electrode exchanging strategy was adopted in this work; in other word, the anode and cathode for electrocatalysis were exchanged after each cycle (30 min). It is expected that the anodic oxidation of RuO_2-TiO_2 composites in the previous cycle can be recovered by acting as a cathode in the next cycle. Fig. 9B, D and F show that the activity reproducibility of the
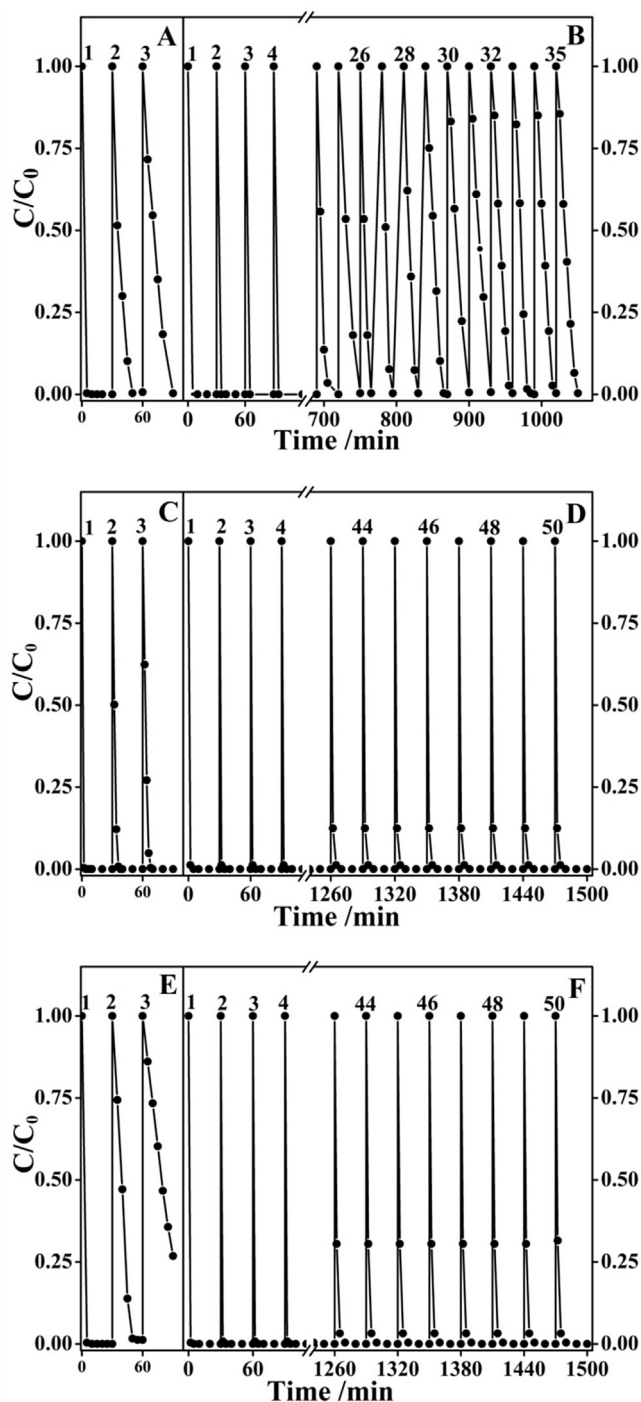
Fig. 9. Repeated tests for the removal of nitrite with (A, B) 0.1 wt% RuO$_2$-TiO$_2$/Ti, (C, D) 2.0 wt% RuO$_2$-TiO$_2$/Ti, and (E, F) RuO$_2$/Ti. Left side (A, C, E): continuous test without exchanging the anode and cathode; right side (B, D, F): exchanging the anode and cathode after every cycle (30 min).

Fig. 10. The 2 min nitrite removal rate with (a, b) anode and cathode exchanging, and (c, d) anode and cathode non-exchanging. Electrodes: (a,c) 2.0 wt% RuO$_2$-TiO$_2$/Ti, (b, d) RuO$_2$/Ti.

cycles for 0.1 wt% RuO$_2$-TiO$_2$/Ti, 2.0 wt% RuO$_2$-TiO$_2$/Ti and RuO$_2$/Ti, respectively.

Fig. 10 summarizes the electrochemical service life of the 2.0 wt% RuO$_2$-TiO$_2$/Ti electrode and RuO$_2$/Ti electrode. It shows that the electrochemical performances of 2.0 wt% RuO$_2$-TiO$_2$/Ti electrode and RuO$_2$/Ti electrode deteriorated quickly if they were merely used as anodes; the nitrite removal rates in 2 min decrease to less than 50% for both electrodes after reused twice. Fortunately, by introducing the electrode exchanging strategy, both 2.0 wt% RuO$_2$-TiO$_2$/Ti and RuO$_2$/Ti show a much extended lifetime for their electrocatalytic applications. As the RuO$_2$ are the predominantly electrocatalytically active species for producing active chlorine species [24,25], RuO$_2$/Ti electrode gives a competitive activity for nitrite removal at the initial cycles. Nevertheless, the catalytic activity life of RuO$_2$/Ti electrode seems not as good as that of 2.0 wt% RuO$_2$-TiO$_2$/Ti electrode. As is shown in Fig. 10, the 2 min removal rate of nitrite with the 2.0 wt% RuO$_2$-TiO$_2$/Ti electrode almost keeps the perfect performance even after 50 cycles. However, that with the RuO$_2$/Ti electrode obviously decreases: the 2 min removal rate of nitrite gradually slows down from 99.8% to 63.3%. The better activity and reproducibility of 2.0 wt% RuO$_2$-TiO$_2$/Ti electrode should be attributed to the interaction of RuO$_2$ with TiO$_2$, which stabilizes the chemical states of RuO$_2$ during the electrocatalysis process.

To sum up, by regularly changing the positive and negative polarities of the RuO$_2$-TiO$_2$/Ti electrode, the problem of electrode passivation can be effectively eliminated. The 2.0 wt% RuO$_2$-TiO$_2$/Ti electrode owns superior activity and excellent stability, which beneficial for their further applications.

3.6. The mechanism of the removal of nitrite

Owing to the detection limits of the ion selectivity electrodes for the generated N-species (PNO$_3$-1-01: 10^{-1}–10^{-5} M, PNH$_3$-1: 10^{-1}–5 × 10^{-6} M), a sodium nitrite concentration of 110 mg L^{-1} was used for aqueous N-species analyses. 0.05 M NaCl or 0.0167 M Na$_2$SO$_4$ (with the same ionic strength) was added in reaction solution to compare the impact of different supporting electrolytes. The presence of chloride ion has a little influence to the apparent potential of the PNO$_3$ electrode at low nitrate concentrations, therefore, the calibration curve of nitrate ion was made for eliminating the influence of chloride ion (Fig. S4). The temporal changes of nitrite, nitrate, ammonia and the total content of N (Total-N) are presented in Fig. 11. For the ease of comparison, all the N-species concentra-

electrode was largely enhanced for the nitrite removal. Comparing with Fig. 9A and B, the electrocatalytic efficiency of the 0.1 wt% RuO$_2$-TiO$_2$/Ti electrodes improved after adopting the exchanging strategy, a complete removal of nitrite can be achieved in 5 min at the earliest 3 cycles. Similarly, 2.0 wt% RuO$_2$-TiO$_2$/Ti electrode and RuO$_2$/Ti electrode (containing same amount of RuO$_2$ amount with that of 2.0 wt% RuO$_2$-TiO$_2$/Ti electrode) show much enhanced activity reproducibilities with the electrode exchanging strategy. Completely removals of nitrite were observed after 35, 50 and 50
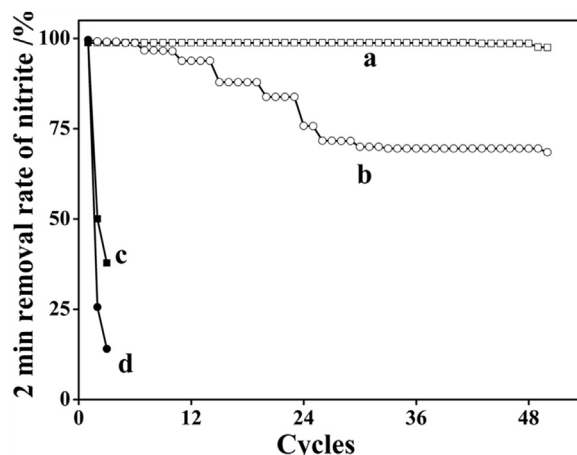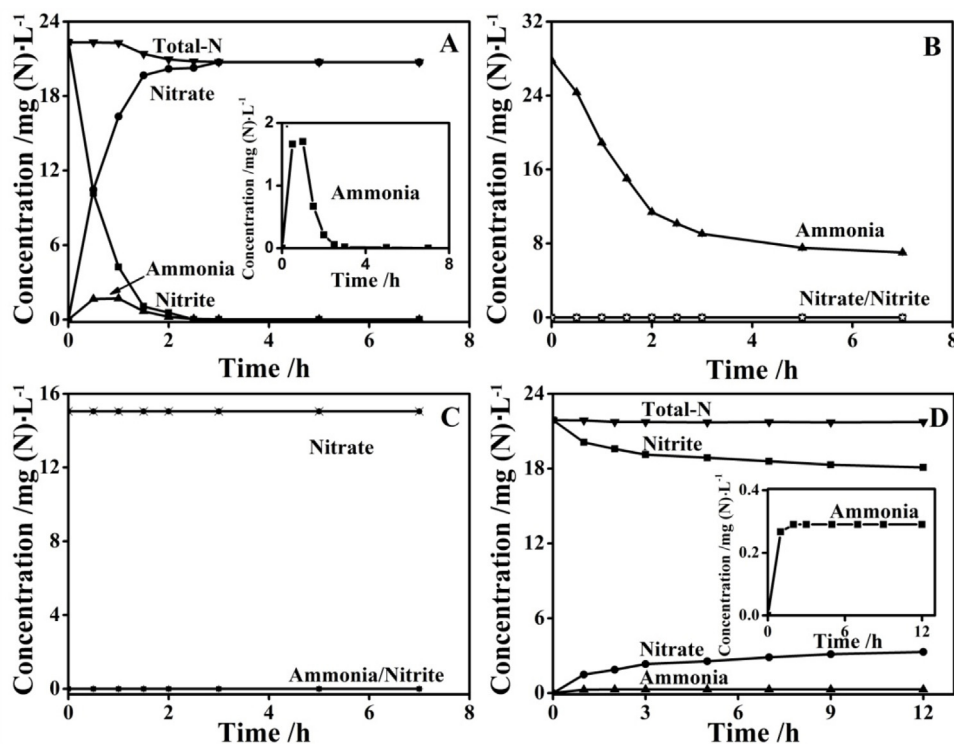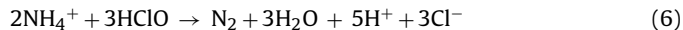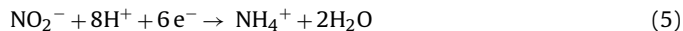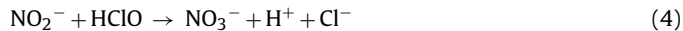
Fig. 11. N-species evolution during the electrocatalysis with RuO_2-TiO_2/Ti electrodes for (A) the initial solution contains $110\,mg\,L^{-1}$ $NaNO_2$, 0.05 M NaCl; (B) the initial solution contains $110\,mg/L$ NH_4Cl, 0.05 M NaCl; (C) the initial solution contains $110\,mg\,L^{-1}$ KNO_3, 0.05 M NaCl; and (D) the initial solution contains $110\,mg\,L^{-1}$ $NaNO_2$, 0.0167 M Na_2SO_4.

tions were recorded according to the corresponding weight content of N element.

Generally, the addition of desired electrolyte into the reaction solution can enhance the electrocatalytic efficiency by improving the conductivity. Fig. 11A presents the temporal changes of N-species during the electrochemical removal of nitrite in the presence of NaCl. All the nitrite ($22.3\,mg(N)\,L^{-1}$ NO_2^-) are eliminated in ca. 2.0 h, while nitrate and ammonia appear as the products. The produced ammonia, however, reaches the maximum ($1.7\,mg(N)\,L^{-1}$) at ca. 1.0 h, and then stepwise disappears. According to the amount changes of the total-N, the ammonia-N seems to be released from the reaction solution. In order to verify this assumption, the electrochemical reaction was copied except that NH_4Cl was used as the initial species. Ammonia decreases from $27.8\,mg(N)\,L^{-1}$ to $7.0\,mg(N)\,L^{-1}$ in ca. 7.0 h. Along with the disappearance of ammonia, no nitrite or nitrate ions are observed as shown in Fig. 11B. Put it another way, the oxidation of ammonia is most responsible for the total-N elimination in the reaction solution, while nitrate is presented as the dominant product in the electrochemical elimination of nitrite. Besides, the nitrate seems to be pretty stable in this system in the presence of NaCl. To confirm this phenomenon, another similar experiment was conducted, in which KNO_3 was chosen as the initial species (Fig. 11C). Throughout the entire ca. 7.0 h electrolytic process, neither ammonia nor nitrite is detected, and no decrease of nitrate is observed. That is to say, the nitrate reduction cannot be achieved for RuO_2-TiO_2/Ti electrodes in this condition. As is known, the chloride ions are involved in the electrochemical process by losing one electron at the anode to give chlorine molecule, as that shown in Fig. 6. Therefore, Na_2SO_4 is chosen as an alternative inert electrolyte to recognize the contribution of chloride in this work. As shown in Fig. 11D, nitrate and ammonia species are also generated, but in a much slower manner. Only $3.7\,mg(N)\,L^{-1}$ (17.0%) of the nitrite is transformed in 12 h, of which $3.3\,mg(N)\,L^{-1}$ is oxidized into nitrate whereas the rest 0.4

$mg(N)\,L^{-1}$ is reduced into ammonia. However, the conversion of nitrite in 3.0 h (Fig. 11A) reaches 100% with the addition of NaCl, in which 92.3% of the nitrite is oxidized into nitrate.

Moreover, in NaCl aqueous solution, an indirect oxidation by hypochlorite during electrocatalysis process is suggested at the anode. Meanwhile, the cathode product of nitrite reduction would also produce ammonium ions [45]. In the presence of chloride ions (Cl^-), the electrochemical reaction at anode leads to chlorine molecules formation, which immediately reacts with water and hypochlorite produced afterwards [3,46]. The hypochlorite then plays the dominated role in nitrite and ammonia oxidizing process. These reactions in solution are as follows [45–49]:

$$2Cl^- \rightarrow Cl_2 + 2e^- \tag{1}$$

$$Cl_2 + H_2O \rightarrow HClO + H^+ + Cl^- \tag{2}$$

$$HClO \rightarrow ClO^- + H^+ \tag{3}$$

$$NO_2^- + HClO \rightarrow NO_3^- + H^+ + Cl^- \tag{4}$$

$$NO_2^- + 8H^+ + 6e^- \rightarrow NH_4^+ + 2H_2O \tag{5}$$

$$2NH_4^+ + 3HClO \rightarrow N_2 + 3H_2O + 5H^+ + 3Cl^- \tag{6}$$

4. Conclusions

A surface modification method was used to synthesize the RuO_2-TiO_2/Ti electrode. RuO_2 nanoclusters form epitaxial layers on the surface of TiO_2 under 400 °C calcination, which gives a significant promotion in electrochemical properties of RuO_2-TiO_2/Ti electrode: lower impedance and better electrocatalytic activity. With the increasing of loaded RuO_2 content from 0 to 2.0 wt%, the electrocatalytic activity of the RuO_2-TiO_2/Ti electrode is greatly increased. The nitrite removal rate of 2.0 wt% RuO_2-TiO_2/Ti electrode is ca. 6.7 and 2.5 times faster than those of 0.02 wt% and 0.1 wt% RuO_2-TiO_2/Ti electrodes, respectively. By exchanging the

anode and cathode after every reaction cycle (30 min) to recover the oxidation of RuO_2 active sites, the catalytic activity of corresponding 2.0 wt% RuO_2-TiO_2/Ti electrode doesn't decrease obviously after 50 cycles. Although the electrocatalytic service life of RuO_2/Ti electrode is also greatly improved, its electrocatalytic activity decreases much after 50 cycles. The relatively longer service life of 2.0 wt% RuO_2-TiO_2/Ti electrode can be related to the epitaxial spread of RuO_2 on the surface of TiO_2. The main electrocatalytic product of nitrite-N is nitrate-N by indirect oxidation, while a small amount of ammonia-N also produce from the reduction of nitrite-N at the cathode. In the presence of chloride ion, the RuO_2-TiO_2/Ti electrode oxidizes Cl^- to active chlorine, which oxidizes the nitrite into nitrate. The as-produced ammonia-N intermediate will be oxidized into nitrogen molecule, which is then released from the aqueous solution and leads to the decrease of the total-N in the solution.

Acknowledgement

Appendix A. Supplementary data

Supplementary data associated with this article can be found, in the online version, at http://dx.doi.org/10.1016/j.apcatb.2017.02.005.

References

[1] D. Majumdar, N. Gupta, J. Environ. Health 42 (2000) 28–39.
[2] S.K. Gupta, R. Gupta, A. Gupta, A. Seth, J. Bassin, A. Gupta, Environ. Health Perspect. 108 (2000) 363.
[3] M. Li, C. Feng, Z. Zhang, N. Sugiura, Electrochim. Acta 54 (2009) 4600–4606.
[4] J.-J. Her, J.-S. Huang, Bioresour. Technol. 54 (1995) 45–51.
[5] S.S. Adav, D.-J. Lee, J. Lai, Appl. Microbiol. Biot. 85 (2010) 773–778.
[6] J. Chung, K. Amin, S. Kim, S. Yoon, K. Kwon, W. Bae, Water Res. 58 (2014) 169–178.
[7] A.C. Merkle, N. Lehnert, Dalton Trans. 41 (2012) 3355–3368.
[8] M. Ghazouani, H. Akrout, L. Bousselmi, J. Desalin, Water Treat. 53 (2015) 1107–1117.
[9] H. Särkkä, A. Bhatnagar, M. Sillanpää, J. Electroanal. Chem. 754 (2015) 46–56.
[10] S. Chai, G. Zhao, P. Li, Y. Lei, Y.-n. Zhang, D. Li, J. Phys. Chem. C 115 (2011) 18261–18269.
[11] L.-Å. Näslund, C.M. Sánchez-Sánchez, Á.S. Ingason, J. Bäckström, E. Herrero, J. Rosen, S. Holmin, J. Phys. Chem. C 117 (2013) 6126–6135.
[12] R.M. Asmussen, M. Tian, A. Chen, Environ. Sci. Technol. 43 (2009) 5100–5105.
[13] M. Panizza, P. Michaud, G. Cerisola, C. Comninellis, Electrochem. Commun. (2016) 3.
[14] S. Trasatti, Electrochim. Acta 45 (2000) 2377–2385.
[15] F.A. De Bruijn, V.A.T. Dam, G.J.M. Janssen, Fuel Cells 8 (2008) 3–22.
[16] E. Guilminot, A. Corcella, F. Charlot, F. Maillard, M. Chatenet, J. Electrochem. Soc. 154 (2007) B96–B105.
[17] J.B. Goodenough, A. Hamnett, B.J. Kennedy, R. Manoharan, S.A. Weeks, Electrochim. Acta 35 (1990) 199–207.
[18] P. Michaud, M. Panizza, L. Ouattara, T. Diaco, G. Foti, C. Comninellis, J. Appl. Electrochem. 33 (2003) 151–154.
[19] F. Zhang, C. Feng, W. Li, J. Cui, Int. J. Electrochem. Sci. 9 (2014) 943–954.
[20] Q. Zhuo, S. Deng, B. Yang, J. Huang, G. Yu, Environ. Sci. Technol. 45 (2011) 2973–2979.
[21] V. Sangeetha, V. Sivakumar, A. Sudha, K. Kannan, Int. J. Electrochem. Sci. 10 (2015) 1506–1516.
[22] N. Menzel, E. Ortel, K. Mette, R. Kraehnert, P. Strasser, ACS Catal. 3 (2013) 1324–1333.
[23] Z. Zhang, Titanium Electrode Industry, 2nd ed., Metallurgy Industry Press, Beijing, 2003.
[24] Y. Takasu, W. Sugimoto, Y. Nishiki, S. Nakamatsu, J. Appl. Electrochem. 40 (2010) 1789–1795.
[25] T. Arikawa, Y. Murakami, Y. Takasu, J. Appl. Electrochem. 28 (1998) 511–516.
[26] G.N. Martelli, R. Ornelas, G. Faita, Electrochim. Acta 39 (1994) 1551–1558.
[27] Y. Jiao, H. Jiang, F. Chen, ACS Catal. 4 (2014) 2249–2257.
[28] G.A. Cutter, Anal. Chim. Acta 149 (1983) 391–394.
[29] J. Melsheimer, D. Ziegler, Thin Solid Films 163 (1988) 301–308.
[30] D.-J. Yun, H.-m. Ra, S.B. Jo, W. Maeng, S.-h. Lee, S. Park, J.-W. Jang, K. Cho, S.-W. Rhee, ACS Appl. Mater. Inter. 4 (2012) 4588–4594.
[31] M.T. Uddin, Y. Nicolas, C. Olivier, T. Toupance, M.M. Müller, H.-J. Kleebe, K. Rachut, J. Ziegler, A. Klein, W. Jaegermann, J. Phys. Chem. C 117 (2013) 22098–22110.
[32] R. Schafranek, J. Schaffner, A. Klein, J. Eur. Ceram. Soc. 30 (2010) 187–192.
[33] M. Subhramannia, B.K. Balan, B.R. Sathe, I.S. Mulla, V.K. Pillai, J. Phys. Chem. C 111 (2007) 16593–16600.
[34] L.-Å. Näslund, Aí.S. Ingason, S. Holmin, J. Rosen, J. Phys. Chem. C 118 (2014) 15315–15323.
[35] G. Liu, W. Jaegermann, J. He, V. Sundström, L. Sun, J. Phys. Chem. B 106 (2002) 5814–5819.
[36] G. Xiang, X. Shi, Y. Wu, J. Zhuang, X. Wang, Sci. Rep. 2 (2012) 801.
[37] S. Hoseinieh, F. Ashrafizadeh, M. Maddahi, J. Electrochem. Soc. 157 (2010) E50–E56.
[38] V. Panić, A. Dekanski, V. Mišković-Stanković, S. Milonjić, B. Nikolić, J. Electroanal. Chem. 579 (2005) 67–76.
[39] V.V. Panić, B.Ž. Nikolić, J. Serb. Chem. Soc. 73 (2008) 1083–1112.
[40] S. Hoseinieh, F. Ashrafizadeh, Ionics 19 (2013) 113–125.
[41] X. Chen, G. Chen, Electrochim. Acta 50 (2005) 4155–4159.
[42] F. Hine, M. Yasuda, T. Noda, T. Yoshida, J. Okuda, J. Electrochem. Soc. 126 (1979) 1439–1445.
[43] D. Shao, W. Yan, X. Li, H. Yang, H. Xu, Ind. Eng. Chem. Res. 53 (2014) 3898–3907.
[44] D.T. Cestarolli, A.R. De Andrade, Electrochim. Acta 48 (2003) 4137–4142.
[45] V. Rosca, M. Duca, M.T. de Groot, M.T.M. Koper, Chem. Rev. 109 (2009) 2209–2244.
[46] L. Li, Y. Liu, J. Hazard. Mater. 161 (2009) 1010–1016.
[47] M. Li, C. Feng, Z. Zhang, X. Lei, R. Chen, Y. Yang, N. Sugiura, J. Hazard. Mater. 171 (2009) 724–730.
[48] M. Li, C. Feng, Z. Zhang, Z. Shen, N. Sugiura, Electrochem. Commun. 11 (2009) 1853–1856.
[49] M. Safari, A. Rezaee, B. Ayati, A. Jonidi-Jafari, Res. Chem. Intermediat. 41 (2015) 1365–1372.